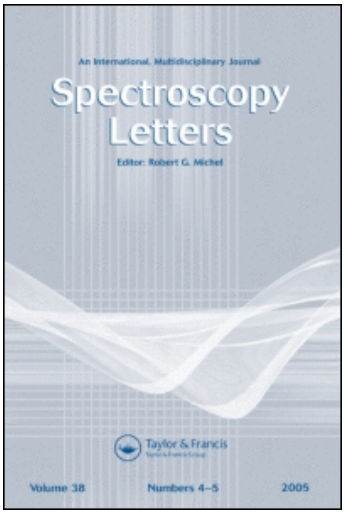

Spectroscopy Letters
Publication details, including instructions for authors and subscription information:
http://www.informaworld.com/smpp/title~content=t713597299

Post-Hoc Vibration Mitigation for Single-Molecule Tracking and Diffusion Measurements in Lipid Membranes

Derek J. Bailey[a]; Jared T. Kindt[a]; M. Madison Taylor[a]; Ashley R. Paulson[a]; Brynna H. Jones[a]; Katie L. Hubbell[a]; Lisa M. Keranen-Burden[a]; Daniel L. Burden[a]
[a] Wheaton College, Wheaton, IL

Online publication date: 20 October 2010

To cite this Article Bailey, Derek J. , Kindt, Jared T. , Taylor, M. Madison , Paulson, Ashley R. , Jones, Brynna H. , Hubbell, Katie L. , Keranen-Burden, Lisa M. and Burden, Daniel L.(2010) 'Post-Hoc Vibration Mitigation for Single-Molecule Tracking and Diffusion Measurements in Lipid Membranes', Spectroscopy Letters, 43: 7, 586 — 596
To link to this Article: DOI: 10.1080/00387010.2010.510734
URL: http://dx.doi.org/10.1080/00387010.2010.510734

Spectroscopy Letters, 43:586–596, 2010

ISSN: 0038-7010 print/1532-2289 online
DOI: 10.1080/00387010.2010.510734

Taylor & Francis
Taylor & Francis Group

Post-Hoc Vibration Mitigation for Single-Molecule Tracking and Diffusion Measurements in Lipid Membranes

**Derek J. Bailey,
Jared T. Kindt,
M. Madison Taylor,
Ashley R. Paulson,
Brynna H. Jones,
Katie L. Hubbell,
Lisa M. Keranen-Burden,
and Daniel L. Burden**

Wheaton College, Wheaton, IL

ABSTRACT Single-molecule tracking algorithms and analyses that use particle trajectory information rely on the accurate determination of particle positions to produce a meaningful interpretation of molecular dynamics. However, artifacts arising from vibration can sometimes distort or entirely mask the processes being studied. Here we describe a straightforward implementation of the Lucas-Kanade stabilization algorithm that can remove the impact of instrument-related vibrations on molecular diffusion measurements after a data set has been collected. Using fluorescently derivatized αHL on supported lipid bilayers in conjunction with computer simulations of 2D diffusion, we report that post-hoc stabilization can be effective in removing both simple and complex noise sources. The effectiveness of vibration mitigation is a function of the relationship between the vibration amplitude and the magnitude of the diffusion constant. For diffusion constants in the range of typical membrane proteins (e.g., 10^{-9} to 10^{-7} cm^2s^{-1}), vibrations that produce errors in excess of 100% can be reduced to producing errors less than 5%. The algorithm is effective even when the relative magnitude of the vibration is high and can be especially useful in experiments where vibrations cannot be entirely removed by experimental means alone.

Supplemental materials are available for this article. Go to the publisher's online edition of Spectroscopy Letters *for the following free supplemental resources: Video content illustrating single–molecule tracking capability, output from the single–molecule simulator, and the impact of post-hoc vibration stabilization.*

KEYWORDS alpha-hemolysin, image, image stabilization, lipids, Lucas-Kanade, single-molecule simulations, single-particle tracking, vibration, wide-field microscopy

INTRODUCTION

Over the past ~17 years, four main optical approaches to single-molecule fluorescence detection have been explored: near-field scanning optical microscopy,[1–7] confocal fluorescence microscopy (one- and two-photon

Coauthors Derek J. Bailey, Jared T. Kindt, M. Madison Taylor, Ashley R. Paulson, Brynna H. Jones, and Katie L. Hubbell were undergraduates at time of research.

Received 26 August 2009;
accepted 16 December 2009.

Address correspondence to Daniel L. Burden, Wheaton College, Wheaton, IL 60187, U.S.A.. E-mail: daniel.l.burden@wheaton.edu

excitation),[8,9] epifluorescence microscopy,[5,10,11] and total internal reflection fluorescence (TIRF) microscopy.[11,12] The last two approaches utilize an array detector to produce images of a 2D sample, making it possible to track the spatial location of individual molecules as they move and/or diffuse through time. Translational diffusion constants can be computed from the spatial coordinates determined in the tracking analysis. Such measurements have been applied to numerous chemical and biochemical scenarios, including sol-gel materials,[13] diffusion model membranes,[14] ion channels,[15] and especially investigations of cell membrane dynamics.[16] With either approach, there is a need to benchmark idealized measurement conditions so that instrument artifacts can be identified and proper solutions can be engineered. For example, the presence of low-frequency drift in the microscope stage or high-frequency vibrations in the sample and apparatus can distort tracking and diffusion measurements, if not properly mitigated.

Brownian motion creates independent translation among individual molecules in a lipid membrane environment. All molecules, including the labeled molecules, move relative to each other with a non-uniform distribution of step sizes in time and a direction that is not predictable on a molecule-by-molecule basis. Thus, the presence of vibration can be difficult to detect by eye, particularly if the concentration of visible and/or light-producing objects is low and the amplitude of the vibration is small with respect to the displacement arising from Brownian motion. The impact of vibrations on single-particle tracking algorithms and the diffusion constants computed from this information can be significant, particularly if the molecule exists in a highly viscous or constrained local environment.

The problematic effects of high-frequency vibration can be lessened by using acoustical enclosures: levitated optical benches with massive tops: rigid mechanical supports for the equipment; and rigorous heating, ventilation, and air conditioning (HVAC) control in the laboratory (to lessen air pressure oscillations from rotating fans). However, in some laboratory environments these countermeasures can be expensive and difficult to exhaustively and effectively implement.

Here, we evaluate the idea of using digital image stabilization to remove vibrations in single-molecule tracking and diffusion experiments post-hoc. To assist in the task, we use a computer simulation that models the photophysical and translational dynamics of point particles moving in a 2D plane and that closely mimics data acquired from an epi-illuminated, wide-field, single-molecule fluorescence microscope. This permits exploration of a version of the Lucas-Kanade[17,18] image stabilization algorithm, which calculates a geometric transformation to align future frames in an image series with a reference frame, or template. The particular version of the algorithm we utilize (written by Kang Li) adjusts this frame of reference as time progresses and is available as a plug-in to the ImageJ software package.[19] "On-the-fly" modification of the template is performed by computing a weighted average of the previous template and the frame being aligned. This process is repeated so that each successive frame in the time series of images is aligned to a modified template. In this manner, the reference frame always remains localized in time to the frame being stabilized. This process is particularly amenable to image sequences that contain random or independently moving objects, such as Brownian motion in model lipid membranes or the membranes of living cells. In addition, its availability as a freeware plug-in to ImageJ makes implementation simple and inexpensive.

MATERIALS AND METHODS

Production of Fluorescently Labeled αHL

We use measurements of fluorescently labeled proteins diffusing in a lipid membrane environment as a benchmark for the development of computer simulations. Alpha-hemolysin (αHL) protein was produced and labeled in our laboratory. For this, a pair of DNA primers with a mutation site designed to replace the amino–acid at the 244th position with cysteine was constructed and combined with a plasmid template containing wild type αHL in a polymerase chain reaction (QuikChange Site-Directed Mutagenesis Kit, Stratagene, La Jolla, CA). Mutant protein αHL-N244C with an N-terminal His_6 affinity tag was expressed in *E. coli* (BL21, Novagen, Gibbstown, NJ) and purified by immobilized metal affinity chromatography (IMAC) using HisTrap resin

(GE Healthcare, Piscataway, NJ) to greater than 97% purity as judged by SDS-PAGE at 1–15-μM concentrations as previously described.[20]

A 10X molar excess of thiol-specific Alexa Fluor 532 (Invitrogen, Carlsbad, CA) in DMSO was reacted with purified αHL-N244C (12.5 μM) for 2 hr at 25°C. Unreacted free dye was removed from the fluorescently labeled αHL-N244C-A_{532} using IMAC with protein eluting upon addition of 400-mM imidazole. The αHL-N244C-A_{532} was incubated (4°C for 5 days) with the site-specific protease AcTEV (Invitrogen) to allow removal of the N-terminal His_6 affinity tag (4°C for 5 days) followed by further purification using IMAC. Fully processed αHL-N244C-A_{532} flowed through the column while contaminating His_6-tag, protease, and uncleaved αHL bound to the resin. Highly purified, fluorescently labeled αHL (~0.1 mg/ml) was stored in 20-mM Tris (pH 7.5), 100-mM KCl at 4°C.

Experiments in Supported Membranes

Supported lipid membranes were formed on a glass surface following a version of the vesicle fusion technique reported by Tamm.[21] All microscope slides and glass vials were cleaned in piranha solution (3:1 H_2SO_4/30% H_2O_2) and rinsed with ddH_2O. The microscope slide was allowed to air dry in a covered container, and the vials were dried under vacuum. A 25 × 25 × 2–mm rubber gasket (Grace Bio-Labs) was applied to the microscope slide. Lyophylized lipids (*N*-(6-tetramethylrhodaminethiocarbamoyl)-1,2-dihexadecanoyl-*sn*-glycero-3-phosphoethanolamine (DHPE) and 1,2-Diphytanoyl-*sn*-Glycero-3-Phosphocholine (DØPC) were purchased from Avanti Polar Lipids and Invitrogen, respectively. Lipid mixtures containing 0–1 mole% DHPE:DØPC were created from chloroform (Sigma–Aldrich, St. Louis, MO) stocks and transferred into a cleaned vial (total of 5 mg/mL of lipid). The chloroform was allowed to evaporate under vacuum for 20 min, and the lipid was resuspended in 30 μL of isopropanol. To spontaneously form vesicles, the isopropanol solution was injected into 5 mL of Tris-buffered saline (TBS) solution (10-mM Tris pH 7.5, 100-mM NaCl), while rapidly vortexing for 90 s. The vesicle solution was then transferred on to the microscope slide and incubated for 2 hr. Following the incubation and deposition period, the solution was gently exchanged with TBS for 15 min using a peristaltic pump. As reported previously,[22] this procedure, when performed with 1% fluorescent lipid (DHPE), shows a uniform fluorescent layer on the glass surface. This indicates successful formation of a homogeneous lipid bilayer. Following solution exchange, 10 μL of a fluorescent αHL solution (2-M KCl, 500-nM N244C-A_{532}) were injected on top of the bilayer and incubated for 1 hr in darkness. The membrane was then washed with TBS solution for 10 min before we acquired optical data.

Wide-Field Microscopy

All single-molecule tracking videos were collected using a modified upright Axiotech Vario microscope (Carl Zeiss, Inc., Thornwood, NY) secured to a levitated optical table (Technical Manufacturing Corp., Pearland, MD). The microscope chassis was situated above a 3D translation stage and a piezoelectric stage (both Melles Griot, Rochester, NY), which are used to position the sample under the microscope body. The chassis was supported with multiple vertical support beams. Sample illumination was provided by a 2 W, 50-MHz, 532-nm, acousto-optically modulated laser (RAPID, Lumera Laser, Kaiserslautern, Germany), which was coupled to the microscope using a single-mode optical fiber (OZ Optics, Ottawa, Canada). Upon exit from the fiber, the laser light is collimated and refocused to the back aperture of an epiplan-apo water-immersion objective (150x, N.A. = 1.25, Carl Zeiss, Inc., Thornwood, NY) using a focusing lens (AC254–150-A1, Thor Labs, Newton, NJ). Fluorescent photons produced by the laser excitation are collected by the same objective, passed through an emission filter (590WB45, Omega Optical, Brattleboro, VT), and impinge on a frame-transfer EMCCD camera (iXon +897, 512 × 512–pixel array, Andor Technology, Belford, N. Ireland). A mask placed in front of the camera limits the exposed area of the CCD chip to a 90 × 90–pixel sub-region immediately adjacent to the frame-transfer region. This permits frame readout rates of ~500 Hz. Videos were collected at 3-ms and 10-ms exposures for 500–1000 consecutive frames. The microscope (Fig. 1) is housed in an acoustical enclosure to shield from external disturbances. While the apparatus is capable of excluding all measurable vibration noise sources, controlled exposure to

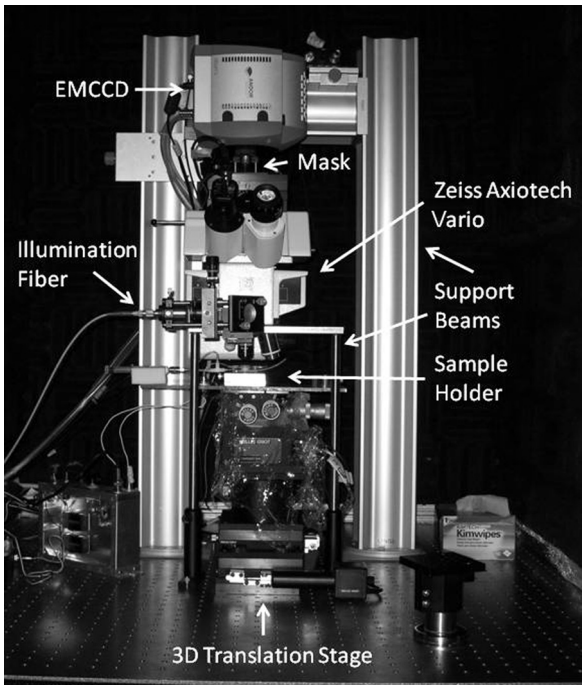

FIGURE 1 **A modified upright epi-fluorescent microscope used for wide-field single-molecule tracking experiments. The microscope is secured on an optical table and is further isolated from external disturbances via an acoustical enclosure.**

inherent acoustical and mechanical noise in the laboratory was permitted either by removing the support beams from the chassis or by not levitating the optical bench.

Single-Molecule Simulations, Particle Tracking, and Trajectory Analysis

Software for running single-molecule simulations was written in Java and operates as a plug-in to the freely available ImageJ software suite. The single-molecule simulator (SMS) runs numerical simulations of 2D diffusing particles and provides a visual representation of the data that can be manipulated to mimic a wide range of experimental conditions. The particle's step size (Δr) is constant and is determined from the user-specified diffusion constant (D) and step time (Δt) using the 2D diffusion relationship:

$$\Delta r = \sqrt{4D\Delta t} \tag{1}$$

The direction of each step is determined by sampling a uniform distribution between 0 and 2π using the MRG32k3a ($\rho = 2^{191}$) pseudorandom number generator. Usually Δt is chosen so that many thousand steps are taken during one simulated frame exposure time (3–10 ms). When Δt is set in the range of 5 μs, 600–2000 steps are taken. Thus, a distribution of step distances and step directions are established for every molecule between each consecutive frame in a manner that approximates true random motion. Importantly, the SMS also provides easy access to an historical record of the X-Y coordinate locations of the simulated point molecules. This feature is used for adding noise sources to the trajectory streams.

Although the molecules move in 2D, the edges of simulation space are connected via wrapping rules; thus a diffusing molecule experiences translation on a virtual 3D torus. A user-specified photon-detection area is situated in the center of simulation space, which creates so-called "dark" regions flanking all sides of the detection area. No photons are produced when molecules move into these dark regions; nevertheless, the algorithm continues the diffusive motion. The dark-buffering region allows moving molecules to effectively experience an infinite translational area, while protecting the photon-detection area from undesired border and wrapping artifacts. It also allows additional particles to diffuse into the detection area over time, which mimics the experimental data.

The spatial distribution of photons detected from an individual molecule is diffraction limited and follows an Airy disk pattern. The width of this disk is determined by the objective numerical aperture (NA) and mean wavelength of fluorescence collection. To simulate this pattern of photon deposition on a CCD array, we distribute photons across a simulated surface by randomly sampling from a 2D Gaussian probability distribution. The centroid of the distribution matches the position of a simulated point particle and has a width that is adjusted to equal the calculated diffraction-limited spot size. Photons, which are represented using integer values, are then randomly deposited in a 2D region that extends 3 standard deviations around the centroid. The number of photons collected is based on the particle's illumination rate and the duration of the time step. Once the end of a frame exposure period has been reached, the photon counts produced by all the simulated point particles in the detection area are compiled into a single image and saved. The process then repeats itself 500–1000 times to create a simulated video output sequence.

Simulated background levels are generated to match the experimentally observed background intensity distribution. For this, a combined Gaussian and exponential probability distribution is required. The ratio of random samples taken from each of the two distributions is determined by the user. The user also specifies the mean and standard deviation of the Gaussian, as well as the decay constant for the exponential. All background counts are limited to a value greater than a specified absolute minimum. Background counts are added to each pixel in the simulated detection area after the fluorescent spots for all simulated particles in that frame have been formed.

During a simulated frame exposure time, each particle in the detection area emits a number of photons that is calculated from a user-specified average emission intensity. Variations on the frame-to-frame intensity are determined by sampling from a Gaussian distribution and follow a user-determined level of variance. The SMS permits adsorption and desorption of molecules from the simulation plane, which simulates a dynamic equilibrium between the surface and aqueous solution. Photobleaching rates can also be specified. Multiple species of molecules can be created, each with a distinct intensity, intensity variation, diffusion constant, and photobleaching rate. Molecules can be made to suddenly change diffusive behavior to simulate entrance or exit from confined states or tight adsorption/desorption events. However, since the primary purpose of this study is to evaluate the potential of post-hoc image stabilization for freely diffusing molecules, these additional simulation features were not explored in detail.

Video sequences of fluorescent αHL and simulated diffusion are analyzed by a modified version of ParticleTracker (PT) written by Guy Levy,[23] which is available as a plug-in for ImageJ. This routine implements the feature point detection and tracking algorithm,[24] which determines the centroid location of each fluorescent spot in each frame and provides frame-to-frame linking analysis so that spots can be tracked as they move in time. Example trajectory output from PT is included in the supplemental information (S1). The PT settings found to be most useful in our analysis were (a) particle radius of 3 pixels, (b) threshold level equal to 4 times the standard deviation of the background (as calculated from the restored image), (c) link range of 1, and (d) frame-to-frame displacement of 5 pixels. Calibrated pixel sizes (105 nm/pixel side) and frame exposure times (3–10 ms) matched the configuration of the microscope and simulations. The modified PT also implements various trajectory-filtering routines to remove spuriously formed trajectories that are shorter than a specified minimum length (e.g., <4 frames), leaving only the longest and most reliable molecular trajectories available for analysis. Our version of PT also generates a tabular trajectory history for spots as they diffuse from frame-to-frame, which can be readily compared to the X-Y coordinates produced by SMS. Since PT empirically analyzes the output data stream, a slight error is introduced in comparison to the locations of particles produced by the SMS.

We also developed a trajectory analysis program (TAP) to analyze the 2D trajectory information generated by PT. The TAP permits calculation of mean squared distances, average particle displacements, and diffusion constants according to previously published methods.[25–30] Specifically, we configured TAP to perform a mean-square displacement analysis of spots in adjacent frames with a lag time (N_d) equal to one.[31] The accuracy of the methodology was confirmed by comparing user-input diffusion constants to output from the TAP. In addition, the TAP also reports the mean molecule displacement (MSD) between subsequent frames as a function of frame number (or time). Given only random diffusive motion of the molecules, this average will normally be close to zero; however, when vibrations are present, a systematic shift away from the average can be identified. This time series output is then made available for analysis via Fourier transformation.

Image Construction, Vibration, and Stabilization

All simulations were run with a 90×90–pixel detection area and an average of 20 particles. Each pixel represents 105 nm in sample space; thus the total area of an image frame is $\sim 90\,\mu m^2$. For determining the potential of the Lucas-Kanade stabilization routine, only one class of diffusing species was modeled, and all molecules within a given simulation were assigned the same diffusion constant. For

vibration studies, duplicate simulations were performed using identical user-input settings, and vibrations were added to one of the output data sets. This allows a direct comparison and the impact of vibrations can be accurately assessed. The vibration patterns added to the particle diffusion simulations were produced in one of two ways: (1) numerical generation of a simple sinusoid waveform with a user-specified frequency, amplitude, and sampling interval, (2) more complex vibrations were experimentally recorded by exposing our apparatus to excessive noise sources.

After vibration was added, the image sequences were stabilized with the modified Lucas-Kanade algorithm. We used a template update coefficient of $\alpha = 0.4$, where α describes the relative weight assigned to old and new frames [new template = α(old template)+(1-α)(last aligned frame)]. The resulting stabilized image sequence was output into a new file. Data simulated without added vibration served as a reference for comparison.

RESULTS AND DISCUSSION

Approximating Experimental Data

To test the Lucas-Kanade algorithm, we first adjusted computer simulation input parameters to replicate the data collected from actual measurements of fluorescently labeled αHL interacting with a fluid lipid membrane supported by a glass microscope slide. The wide-field, epi-fluorescence apparatus used for these measurements is shown in Fig. 1. Sample slides were immersed in water and a water-immersion objective was positioned to within the focal length of the objective (~150 μm). Images from the microscope reveal tightly formed spots only when the sample is within ~1 μm of the focal plane. Fluorescent molecules located in solution above the membrane move too quickly to create spots that can be tracked by the PT software. Thus, detection is generally selective for fluorescent species located on or near the membrane surface. Adsorbed proteins diffuse in two dimensions across the surface of the slide, producing fluorescent spots in consecutive frames. However, in an experimentally acquired video, fluorescent spots occasionally appear or disappear in the middle of the field of view. We ascribe this phenomenon to three possible mechanisms: (1) photobleaching, which causes an irreversible loss of a spot, (2) a dynamic adsorption–desorption equilibrium existing between the lipid bilayer and the surrounding solution, (3) molecules that fluctuate in and out of non-fluorescent states (i.e., molecular blinking). While the simulator input parameters can be adjusted to mimic these phenomena, there was no need to explore these features for the purposes of this study.

Figure 2A shows an all-points histogram and a single-frame image extracted from a 1000-frame video sequence of αHL diffusing on a lipid membrane. Each bright spot shown in the image corresponds to a labeled αHL. Output from a

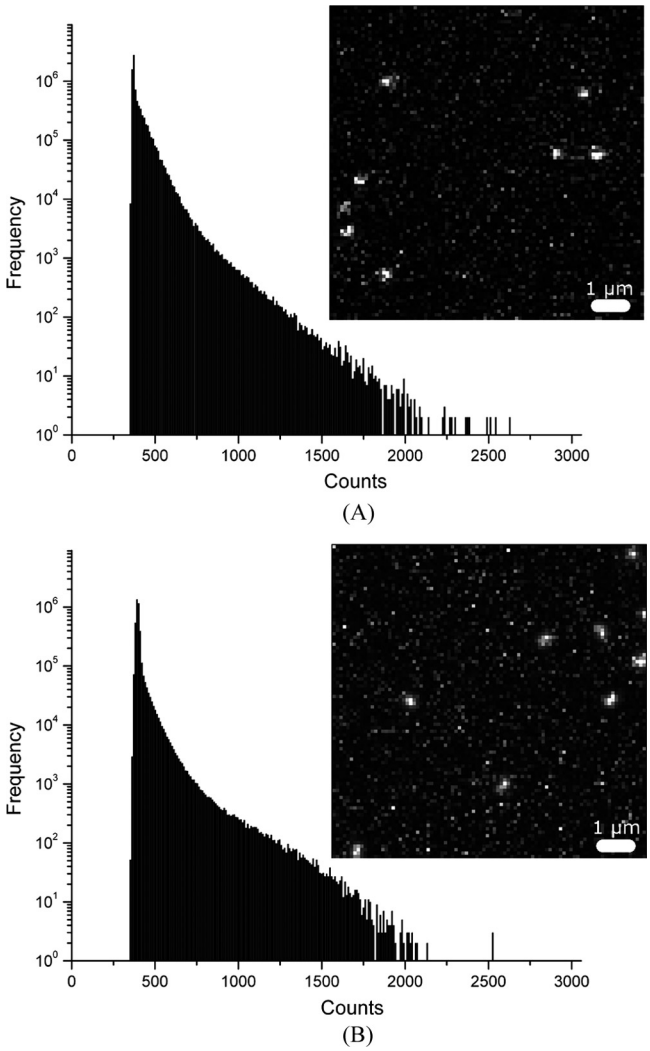

FIGURE 2 **Comparison of real and simulated single-molecule tracking videos. Single-frame snapshots of (A) fluorescently labeled αHL on a supported planer bilayer and (B) simulator output adjusted to mimic the real data. Count histograms constructed from all pixels in all frames (90 × 90 pixels, 1000 frames). See supplements S2 & S3 for video files.**

computer simulation that was adjusted to closely match that of the experiment is shown in Fig. 2B. Video files for both scenarios can be found in the supplemental information (S2 and S3). Histograms carry information from the readout noise of the camera, detected background fluorescence and scattered photons, as well as the spot intensity distribution. As can be seen, the output from the computer simulation closely mimics the actual data. Spot intensity, surface concentration, and trajectory length were all consistent with experimental observations, allowing studies of vibration mitigation on freely diffusing molecules to proceed.

Vibrational Noise

We added vibrational motion to simulated video output files in one of two ways. One approach involved first exposing the apparatus shown in Fig. 1 to controlled levels of acoustical and mechanical noise that are inherently present in the laboratory (e.g., HVAC noise) and recording the induced oscillations in the microscope. Oscillations were recorded for either (1) a small and stationary pinhole defect on the surface of an opaque trans-illuminated air force target or (2) stationary fluorescent spots created by depositing single molecules of labeled αHL on the surface of a bare glass slide. Videos were collected for 500 frames, and PT was used to determine the X-Y coordinates of the non-diffusing spots through time. The measured displacements of these stationary features were then added to the X-Y centroid locations of simulated molecules undergoing pure diffusion. This approach provides a way to closely approximate vibrational interferences that might be present in a real experiment. These oscillations are generally complex due to time-dependent resonances within the structure of the microscope. A second feature in the simulation software allows the user to add pure sinusoidal oscillations at a specified frequency and amplitude for both X and Y directions. We adjusted the peak-to-peak amplitude of the pure sinusoid to be larger than the vibration amplitude acquired in the experiment in an effort to evaluate the Lucas-Kanade algorithm over a range of possible conditions.

Translational and Spectral Analysis

Apparatus vibrations don't typically occupy a single frequency band or possess a uniform amplitude over time. Complex patterns often emerge due to

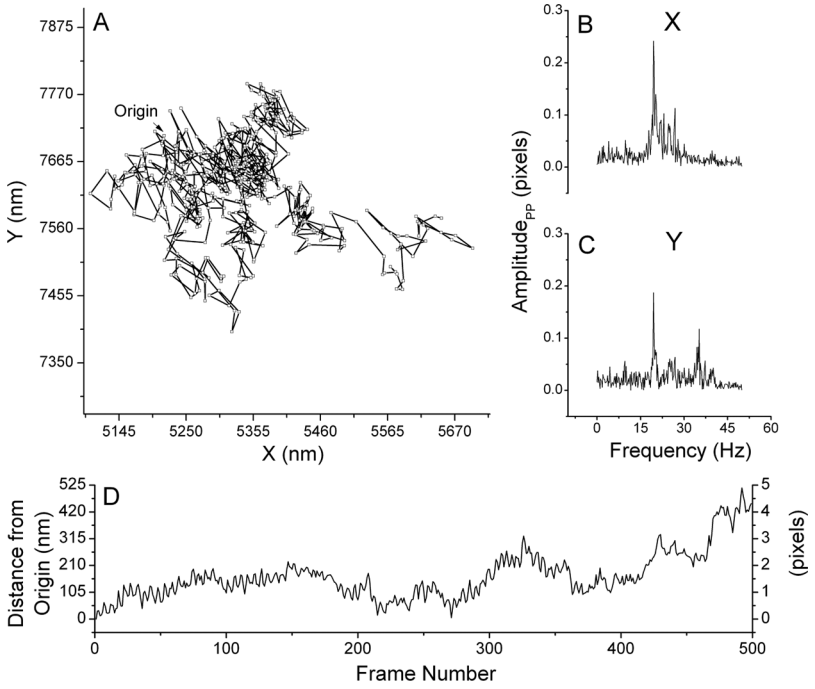

FIGURE 3 **Vibrations recorded from a stationary image feature when the microscope is exposed to excessive room noise. The resulting 2D trajectory (A) gives information on the size and direction of the applied vibration. Spectral analysis (B) and (C) of the X and Y coordinate displacements over time are given in units of pixels. The actual distance the particle moves from its origin (D) varies over time, demonstrating that the vibrations encountered during experiments are dynamic in both time and space. Frame exposure time is 10 ms.**

constructive and destructive interference that resonate within the apparatus structure at different points in time. Figure 3 shows an example of the vibrational translation acquired from stationary spots when the instrument is exposed to room noise. It is dynamic in both time and amplitude. The 2D trajectory of the stationary particle (Fig. 3A) shows coordinate locations spanning 400–500 nm (~4–5 pixels). The particle's original position is specified and represents the beginning of the time sequence. The frequency and amplitude of vibration can be further characterized by Fourier analysis of the motion in the X and Y directions. Figure 3B and Fig. 3C show frequencies in the range of 15–45 Hz. The major peak near 20 Hz in both X and Y spectra can be attributed to the laboratory's HVAC systems. These vibrations are large enough to significantly hinder diffusion measurements acquired on the millisecond timescale.

Figure 3D shows the distance the stationary particle has been displaced from its origin as a function of time. Small and fast oscillations (i.e., between frames 100 and 150) as well as large, slower movements (frames 400 and beyond) can be identified. Such variations in vibration frequency and amplitude make it difficult to effectively use simple band pass noise-reduction filters because a broad range of frequencies is involved. In addition, fluorescent αHL molecules do not typically last from the beginning to the end of a 500-frame video sequence. Molecular trajectories terminate over a much shorter time interval by one of several processes, including translation out of the field of view, photobleaching, desorption, and blinking. In addition, new trajectories begin late in the sequence due to adsorption, emergence from a dark state, or moving into the field of view. Thus, molecules that are tracked near the beginning of the video sequence experience different type and level of vibration than molecules that are tracked near the end of the sequence. Without a robust stabilization algorithm, the time dependent resonance oscillations could be interpreted as the presence of two types of diffusing species, leading to a false understanding of molecular dynamics or an incorrect picture of surface interactions.

We also performed a spectral analysis of the effectiveness of the Lucas-Kanade algorithm. Two diffusion simulations were run with identical parameters. To one simulation, we added the complex vibration pattern. To another, we added a pure 28-Hz sinusoidal vibration. Each simulation was adjusted to produce 500 frames of output, at 10-ms exposure time, with a particle diffusion constant of

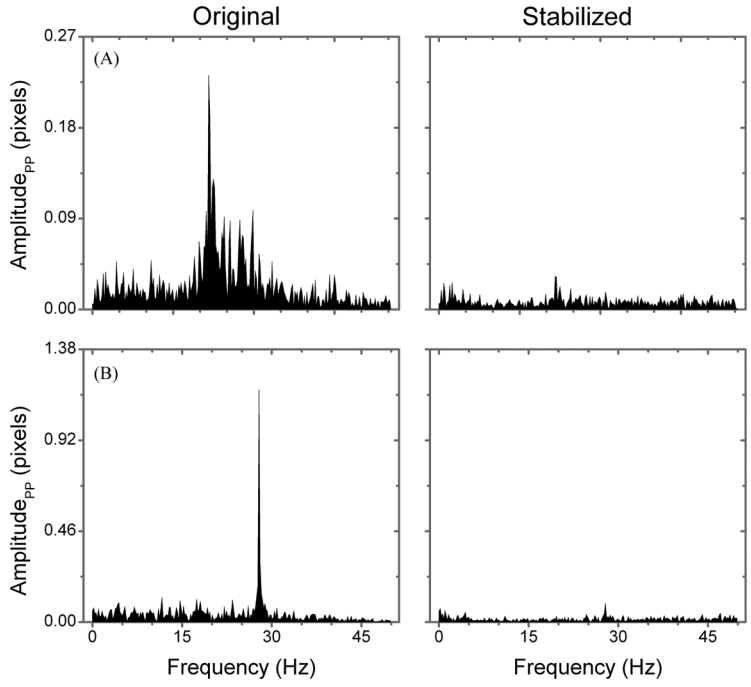

FIGURE 4 **Spectral analysis of Lucas-Kanade algorithm applied to single-molecule tracking simulations before and after stabilization: (A) An 86.3% decrease in the integrated amplitude is observed for complex experimentally acquired vibrations while (B) a 67.9% reduction is determined for the scenario with pure sinusoidal vibration.**

$5.0 \times 10^{-8}\,cm^2s^{-1}$. This is typical of diffusion constants in lipid membranes. Trajectories from each simulation were analyzed, and the average X and Y displacements among molecules was computed. Fourier transformations of the time-dependent average displacements of all particles are shown in Fig. 4. Panels under the "Original" heading show spectral results prior to stabilization. Row A shows results when the complex experimental noise is added, and row B shows results from the application of spectrally pure sinusoidal noise. The Lucas-Kanade algorithm was then applied to each simulation, and the time-dependent average displacements were recalculated. Results from image stabilization are displayed under the "Stabilized" heading. In both scenarios, the Lucas-Kanade algorithm clearly reduces the added noise. In addition, the amplitude of the noise peaks is reduced across all frequencies.

To quantify the level of reduction, we measure the area under the spectral peaks before and after stabilization. Spectral background levels were determined by running a simulation without added noise to produce a relatively flat spectral profile with a slight non-zero value upon integration. The background area was subtracted from each spectra, and the percentage reduction is reported. In the case of the more complex, experimentally derived vibration, we see an 86.3% reduction. In the case of single frequency oscillations, we measure a 67.9% reduction.

Impact on Diffusion Measurement

When vibrations are present, diffusion constant calculations that are based on the molecular trajectories determined by PT can be distorted. This can be particularly problematic if the magnitude of the vibration comprises a significant fraction of the distance a diffusing molecule moves during one frame interval. The simulator allows determination of the error induced by vibration in comparison to the diffusion constant specified by the user. We performed simulations at varying input diffusion constants (1×10^{-9} to $1 \times 10^{-7}\,cm^2s^{-1}$) for 500 frames at 100 Hz. One set of simulations was run with no additional vibration, and the diffusion constant returned by PT and TAP was used as a baseline for percentage error calculations. The same simulations were run a second time with added vibration. Results from the comparison are presented in Fig. 5.

Figure 5A shows simulations having a large amplitude sinusoidal noise source added, while the data in Fig. 5B contain smaller amplitude vibrations induced by exposing the microscope to excessive room noise. The frequency spectra of the noise sources (X-Y directional components), prior to combination with the simulated data, are shown in the inset for reference.

As can be seen, vibration stabilization generally lowers the error in the calculated diffusion constant into the range of 0–10%. Without stabilization, diffusion constant errors rise to 100% or more. Interestingly, for large diffusion constants (i.e., $\sim 10^{-7}\,cm^2s^{-1}$), the presence of vibration does not dramatically interfere with diffusion constant accuracy. In addition, image stabilization at these unaffected diffusion constants does not appear to artificially bias results, as both stabilized and unstabilized data are statistically identical (within the measured uncertainty). Control trials were also performed using vibration-free simulations, where the Lucas-Kanade algorithm was applied to data sets possessing only Brownian motion (data not shown). These experiments determined that in the absence of correlated motion, application of the Lucas-Kanade algorithm did not introduce undesirable bias. Comparison of stabilized and unstabilized data sets produced statistically identical diffusion constant results; thus, Lucas-Kanade selectively reduced vibration over multiple frequency bands, while leaving the random or white noise associated with Brownian motion unaltered.

Figure 5 emphasizes the improvement in accuracy that can be generated by post-hoc stabilization as the diffusion constant decreases. It is interesting to note that the same trend is apparent for both simple and complex noise sources (5A and 5B). However, the more complex noise source generates greater irreproducibility (larger error bars), as would be expected for time-dependent oscillations in multiple directions. Under these conditions, estimating geometric transformations is most likely more difficult for the Lucas-Kanade algorithm. See supplemental files (S4 and S5) for diffusion videos before and after stabilization.

The underlying reason for the separation that grows between stabilized and unstabilized curves relates to the relative amplitude of the vibration in comparison to the average step size taken by diffusing molecules. Figure 6 reveals the affect of the vibration amplitude on the measured diffusion constants. The mean square displacement for

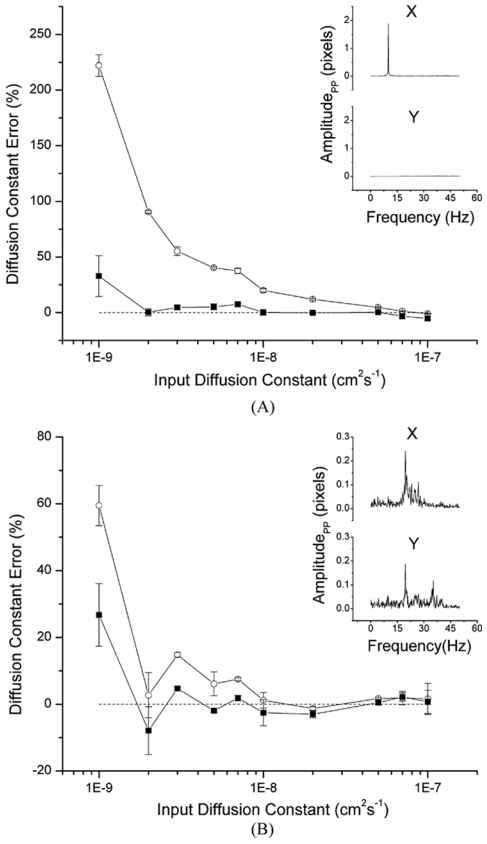

FIGURE 5 **Vibration reduction leads to more accurate diffusion constants. Particles are simulated with a variety of diffusion constants at a fixed 10 ms exposure time. Calculated diffusion constants show significant deviation (○) from the input diffusion constant when idealized (A) and experimental (B) vibration is present. When the Lucas-Kanade algorithm is applied, the calculated diffusion constants (■) are reduced to the level of non-vibrating simulations (———). Error bars represent the standard error of the mean for triplicate measurements.**

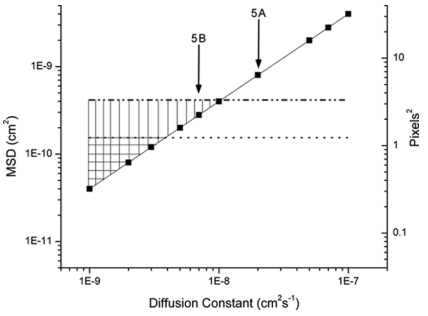

FIGURE 6 **Vibration amplitude in comparison to diffusion step size. (■) Mean square displacements (MSD) of the simulated particles. MSD associated with the sinusoidal vibration displayed in Figure 5a (-●●-) and the experimentally acquired vibration displayed in Figure 5b (●●●). Arrows indicate the diffusion constants in Figure 5 where unmitigated vibration begins to artificially increase the calculated diffusion constants. When vibrations become larger than the molecular motion (hashed regions), the induced error is large. However, the Lucas-Kanade algorithm is able to mitigate the deleterious affect for all but the smallest diffusion constants.**

diffusing species (solid squares connected by line) is calculated for each input diffusion constant at the simulated exposure time of 10 ms using Equation 1. The measured MSDs arising from the two types of added vibration in Fig. 5 are also shown as dashed horizontal lines. These levels were determined by simulating a particle with $D = 0\,cm^2s^{-1}$, adding vibration, and performing a diffusion analysis using PT and TAP. Here, vibrations appear as straight lines since they do not vary with diffusion constant. Both the MSD and the corresponding squared pixel distances on the camera are shown. At large values of D, the vibration amplitude comprises a relatively small fraction of the step displacement. Figure 6 shows that at $10^{-7}\,cm^2s^{-1}$, the experimentally acquired vibration source oscillates with an amplitude that is ~10% of the step distance generated by Brownian motion. It is noteworthy that a measurable level of vibration can be tolerated without introducing significant error. Indeed, when considered together, data from Fig. 5 and Fig. 6 indicate that vibrations for both the large and small amplitude vibration sources will not, on average, disturb diffusion measurements until the peak-to-peak amplitude of the vibration grows to ~50% of the mean squared displacement of the diffusing species. The arrows in Fig. 6 demark the approximate location of a significant rise in error for the unstabilized data sets shown in Fig. 5A and Fig. 5B. As diffusion constants grow smaller, however, the amplitude of the vibration becomes comparable to the movement due to diffusion; thus, the induced error increases for the uncompensated data sets. Figure 5 shows that the Lucas-Kanade algorithm effectively mitigates the impact of vibrations even when the amplitude is considerably larger than the diffusive step distance (hashed regions in Fig. 6). With the exception of the very smallest diffusion constants tested ($1 \times 10^{-9}\,cm^2s^{-1}$), the error remains smaller than 5% for all diffusion constants larger than $\sim 2 \times 10^{-9}\,cm^2s^{-1}$.

CONCLUSIONS

The Lucas-Kanade algorithm is a potentially useful tool for post-hoc removal of problematic vibrations that can arise in single-molecule tracking and diffusion experiments. In this work, emphasis is given to molecules labeled with a single fluorophore; however, application of the stabilization routine need not be

limited. The principles illustrated here could be equally applied to single-particle tracking scenarios employing metal nanoparticles, polymer beads, or quantum dots. In addition, post-hoc stabilization should be applicable to measurement scenarios beyond diffusion in planar lipid membranes. In addition, the Lucas-Kanade algorithm can be effectively used to correct diffusion measurements over a range of diffusion constants. While the exact range of constants will vary depending upon instrumental factors such as magnification, detector pixel size, and the concentration of particles, the principles of relative translation (i.e., vibration amplitude vs. measured particle step distance) remain universal. Vibration stabilization can be effective in situations where the vibration amplitude is up to 5–10 times larger than the particle step distance. Also, post-hoc stabilization does not overtly bias simple diffusion measurements in cases where vibration comprises a relatively small percentage of the overall translation (e.g., 10% or less), or even in cases where no vibrations are present whatsoever. Thus, the algorithm has potential to produce improved results when applied over a large range of diffusion conditions.

ACKNOWLEDGMENTS

Funding for this work has been provided by the National Science Foundation (0550005, 0722688), the American Chemical Society, the Camille and Henry Dreyfus Foundation, Research Corporation, and the Wheaton College Alumni Association.

REFERENCES

1. Betzig, E.; Chichester, R. J. Single molecules observed by near-field scanning optical microscopy. *Science* **1993**, *262*, 1422.
2. Moerner, W. E.; Fromm, D. P. Methods of single-molecule fluorescence spectroscopy and microscopy. *Rev. Sci. Instrum.* **2003**, *74*, 3597.
3. Medina, M. A.; Schwille, P. Fluorescence correlation spectroscopy for the detection and study of single molecules in biology. *Bioessays* **2002**, *24*, 758.
4. de Lange, F.; Cambi, A.; Huijbens, R.; de Bakker, B.; Rensen, W.; Barcia-Parajo, M.; van Hulst, N.; Figdor, C. G. Cell biology beyond the diffraction limit: Near-field scanning optical microscopy. *J. Cell Sci.* **2001**, *114*, 4153.
5. Böhmer, M.; Enderlein, J. Fluorescence spectroscopy of single molecules under ambient conditions: Methodology and technology. *Chemphyschem.* **2003**, *4*, 793.
6. Sako, Y.; Uyemura, T. Total internal reflection fluorescence microscopy for single-molecule imaging in living cells. *Cell Struct. Funct.* **2002**, *27*, 357.
7. Michalet, X.; Kapanidis, A. N.; Laurence, T.; Pinaud, F.; Doose, S.; Pflughoefft, M.; Weiss, S. The power and prospects of fluorescence microscopies and spectroscopies. *Annu. Rev. Biophys. Biomol. Struct.* **2003**, *32*, 161.
8. Nie, S.; Chiu, D. T.; Zare, R. N. Probing individual molecules with confocal fluorescence microscopy. *Science* **1994**, *266*, 1018.
9. Rigler, R.; Mets, U. Diffusion of single molecules through a Gaussian laser beam. *Proc. SPIE Int. Soc. Opt. Eng.* **1992**, *1921*, 239.
10. Schmidt, T.; Schütz, G. J.; Baumgartner, W.; Gruber, H. J.; Schindler, H. Characterization of photophysics and mobility of single molecules in a fluid lipid membrane. *J. Phys. Chem.* **1995**, *99*, 17662.
11. Funatsu, T.; Harada, Y.; Tokunaga, M.; Saito, K.; Yanagida, T. Imaging of single fluorescent molecules and individual ATP turnovers by single myosin molecules in aqueous solution. *Nature* **1995**, *375*, 555.
12. Dickson, R. M.; Norris, D. J.; Tzeng, Y. L.; Moerner, W. E. Three-dimensional imaging of single molecules solvated in pores of poly(acrylamide) gels. *Science* **1996**, *274*, 966.
13. Ye, F.; Collinson, N. M.; Higgins, D. A. What can be learned from single molecule spectroscopy? Applications to sol-gel-derived silica materials. *Phys. Chem. Chem. Phys.* **2009**, *11*, 66.
14. Schütz, G. J.; Schindler, H.; Schmidt, T. Single-molecule microscopy on model membranes reveals anomalous diffusion. *Biophys. J.* **1997**, *73*, 1073.
15. Thompson, J. R.; Heron, A. J.; Santoso, Y.; Wallace, M. I. Enhanced stability and fluidity in droplet on hydrogel bilayers for measuring membrane protein diffusion. *Nano. Lett.* **2007**, *7*, 3875.
16. Wieser, S.; Schütz, G. J. Tracking single molecules in the live cell plasma membrane-Do's and Don't's. *Methods* **2008**, *46*, 131.
17. Lucas, B. D.; Kanade, T. An iterative image registration technique with an application to stereo vision. *Proceedings of the 7th International Joint Conference on Artificial Intelligence*. Vancouver, Canada, **1981**, 674.
18. Baker, S.; Matthews, I. Lucas-Kanade 20 years on: A unifying framework. *International Journal of Computer Vision* **2004**, *56*, 221.
19. Li, K. 2008, http://www.cs.cmu.edu/~kangli/code/Image_Stabilizer.html (accessed July 2009).
20. Chandler, E. L.; Smith, A. L.; Burden, L. M.; Kasianowicz, J. J.; Burden, D. L. Membrane surface dynamics of DNA-threaded nanopores revealed by simultaneous single-molecule optical and ensemble electrical recording. *Langmuir* **2004**, *20*, 898.
21. Tamm, L. K.; McConnell, H. M. Supported phospholipid bilayers. *Biophys. J.* **1985**, *47*, 105.
22. Elliott, J. T.; Burden, D. L.; Woodward, J.; Seghal, A.; Douglas, J. Phospholipid monolayers supported on spun cast polystyrene films. *Langmuir* **2003**, *19*, 2275.
23. MOSAIC Group. ETH Zuirch. http://www.mosaic.ethz.ch/Downloads/ParticleTracker (accessed July 2009).
24. Sbalzarini, I. F.; Koumoutsakos, P. Feature point tracking and trajectory analysis for video imaging in cell biology. *J. Struct. Biol.* **2005**, *151*, 182.
25. Saxton, M. J.; Jacobson, K. Single-particle tracking: Applications to membrane dynamics. *Annu. Rev. Biophys. Biomol. Struct.* **1997**, *26*, 373.
26. Qian, H.; Sheetz, M. P.; Elson, E. L. Single particle tracking: Analysis of diffusion and flow in two-dimensional systems. *Biophys. J.* **1991**, *60*, 910.
27. Schmidt, T.; Shutz, G. J.; Baumgartner, W.; Gruber, H. J.; Schindler, H. Characterization of photophysics and mobility of single molecules in a fluid lipid membrane. *J. Phys. Chem.* **1995**, *991*, 17662.
28. Rudnick, J.; Gaspari, G. The shapes of random walks. *Science* **1987**, 237, 384.
29. Schütz, G. J.; Schindler, H.; Schmidt, T. Single-molecule microscopy on model membranes reveals anomalous diffusion. *Biophys. J.* **1997**, *73*, 1073.
30. Sonnleitner, A.; Schütz, G. J.; Schmidt, T. Free Brownian motion of individual lipid molecules in biomembranes. *Biophys. J.* **1999**, *77*, 2638.
31. Saxton, M. J. Single-particle tracking: The distribution of diffusion coefficients. *Biophys. J.* **1997**, *72*, 1744.